J Mater Sci: Mater Electron (2016) 27:3209–3216
DOI 10.1007/s10854-015-4146-1

CrossMark

Effect of substrate temperature on properties of Cu(In, Ga, Al)Se_2 films grown by magnetron sputtering

Talaat A. Hameed[1,2] · Wei Cao[1] · E. M. Abdelrazek[3] · I. K. El Zawawi[2] · B. A. Mansour[2] · Hani E. Elsayed-Ali[1,4]

Received: 11 July 2015 / Accepted: 26 November 2015 / Published online: 9 December 2015
© Springer Science+Business Media New York 2015

Abstract Cu(In, Ga, Al)Se_2 (CIGAS) thin films were deposited by magnetron sputtering on Si(100) and soda-lime glass substrates at different substrate temperatures, followed by post-deposition annealing at 350 or 520 °C for 5 h in vacuum. Electron probe micro-analysis and secondary ion mass spectroscopy were used to determine the composition of the films and the distribution of Al across the film thickness, respectively. X-ray diffraction analysis showed that the (112) peak of CIGAS films shifts to higher 2θ values with increasing substrate temperature but remains unchanged when the films were annealed at 520 °C for 5 h. Scanning electron microscopy and atomic force microscopy images revealed dense and well-defined grains for both as-deposited and annealed films. However, notable increase in grain size and roughness was observed for films deposited at 500 °C. The bandgap of CIGAS films was determined from the optical transmittance and reflectance spectra and was found to increase as the substrate temperature was increased.

✉ Hani E. Elsayed-Ali
helsayed@odu.edu

1 Applied Research Center, Old Dominion University, 12050 Jefferson Ave., Newport News, VA 23606, USA

2 Solid State Physics Laboratory, Physics Division, National Research Centre, Dokki, Cairo 12622, Egypt

3 Department of Physics, Faculty of Science, Mansoura University, Mansoura 35516, Egypt

4 Department of Electrical and Computer Engineering, Old Dominion University, Norfolk, VA 23529, USA

1 Introduction

Cu(In, Ga)Se_2 (CIGS) and its related compounds are among the most attractive candidates for commercial solar cells because of their high efficiency, long-term stability, and low production costs [1]. The efficiency of CIGS solar cells has exceeded 20 % for laboratory scale devices and up to 15.7 % for commercial modules [2]. CIGS is favorable as an absorber layer because it has a direct bandgap. The bandgap of CIGS changes with the Ga/(In + Ga) ratio and can be tailored between 1.02 and 1.68 eV by varying the Ga/(In + Ga) ratio [3]. In addition, CIGS is well known for its good stability for deposition at relatively high temperatures of 450–590 °C [4]. Another advantage CIGS possesses, as compared to other compound photovoltaic materials, is that it forms a stable phase when its composition significantly deviates from the stoichiometry, i.e., either Cu-poor [Cu/(In + Ga) $<$ 1] or Cu-rich [Cu/(In + Ga) $>$ 1] [5].

It is well known that the performance of CIGS-based solar cells peaks at $\sim$1.2 eV, beyond which the cell efficiency decreases due to increased interface recombination from high defect density when the Ga content is increased [6]. Since a bandgap in the range of 1.4–1.5 eV is desired for better matching to the solar spectrum, efforts have been made to increase the CIGS bandgap while maintaining the device efficiency. One commonly employed approach is to replace some of the elements in CIGS with those from the same group. For example, Gossla and Shafarmann [7] studied $Cu(In_{1-x}Ga_x)(Se_{1-y}S_y)_2$ thin film solar cells and indicated that sulfur increases the bandgap, passivates the surface, and reduces the trap states. Similarly, $Cu(In_{1-x}Al_x)Se_2$ (CIAS) has also been studied as an alternative to CIGS absorber layer in solar cells due to the higher bandgap of $CuAlSe_2$ (2.7 eV) compared to $CuGaSe_2$ [8, 9].

Marsillac et al. [8] deposited CIAS thin films with bandgap varying from 1.00 to 1.52 eV and reported a 16.9 % efficiency for a film with the Al/(Al + In) ratio of 0.13, which corresponds to a bandgap of 1.16 eV. In our previous studies [10, 11], we demonstrated the deposition of single phase Cu(In, Ga, Al)Se_2 (CIGAS) thin films using both pulsed laser deposition and magnetron sputtering. The measured bandgap of CIGAS films increased from 1.22 to 1.47 eV as the Al/(Al + In + Ga) ratio was varied from 0 to 0.4 [11].

Polycrystalline CIGS thin films are deposited by a variety of techniques including thermal evaporation, flash evaporation, spray pyrolysis, electro-deposition, closed-spaced vapor transport, sputtering, and sol–gel [7, 12–18]. A three-stage co-evaporation process was used to fabricate solar cell with the highest efficiencies [19–21]. Co-evaporation relies on how well the flux of each element is controlled during deposition. Additionally, excess residual Se produced in co-evaporation could cause maintenance problems during commercial mass production. Motivated by developing a simple and low cost technique that can be easily integrated into standard semiconductor fabrication, a sputtering process using single quaternary CIGS target has been developed [7, 22, 23].

We have previously reported the deposition of polycrystalline, pure chalcopyrite phase, CIGAS thin films with varying Al content using magnetron sputtering [10]. Since the film quality can be affected by many processing parameters, further studies are needed to optimize the sputtering process. Here, we report on the deposition of CIGAS thin films with fixed Al content using sputtering at various substrate temperatures. The effect of substrate temperature on the chemical composition, structure evolution, and optical properties of the CIGAS films is discussed.

2 Experimental details

Polycrystalline CIGAS thin films were deposited on Si(100) substrates using an ATC Orion-5 magnetron sputtering system (AJA International, Inc., USA) equipped with 2″ sputtering guns and a rotatable heating substrate holder. A 2″ quaternary $Cu_{0.24}(In_{0.20}Ga_{0.06})Se_{0.50}$ target and a 2″ Al target were used for depositing CIGS films and incorporating Al into CIGS, respectively. The base pressure of the sputtering chamber was kept at below 5×10^{-8} Torr and the deposition was performed at 3×10^{-3} Torr with argon (99.999 % purity) at a flow rate of 20 sccm. To add Al, the CIGS sputtering was first carried out using a radio-frequency (RF) sputtering gun operating at 85 W for 30 min. While CIGS sputtering was proceeding, Al was sputtered using a direct current (DC) gun operating at 10 W for 10 min. The CIGS sputtering was then continued for 20 min to result in a film thickness of ~200 nm. The CIGAS thin films were deposited at 25, 150, 250, 350 and 500 °C and then annealed at either 350 or 520 °C for 5 h in vacuum. For optical measurements, all films were also deposited on pre-cleaned soda-lime glass (SLG) substrates using the same process.

The chemical composition of the CIGAS films were determined using a Cameca SX100 (Cameca, France) electron probe micro-analyzer (EPMA). The depth profile of the films was obtained using a TOF-SIMS[5] time-of-flight secondary ion mass spectrometry (TOF-SIMS, ION-TOF GmbH, Germany) with dual beam operation for depth profiling. A 25 keV Bi^+ ion (0.5 pA, 50 μm × 50 μm) for analysis, while a 10 keV Cs ion beam (5 nA, 140 μm × 140 μm) was used for sputtering. Two reproducible depth profiles were acquired for each sample. The crystal structure was studied by x-ray diffraction (XRD, MiniFlex II, Rigaku, Japan) using a CuKα radiation (λ = 1.54 Å) and by high-resolution transmission electron microscopy (HRTEM, JEM-2100F, JEOL, Japan). The TEM specimens were prepared by depositing CIGAS thin films directly on carbon-coated Cu grids using the same deposition conditions described above except for a shorter deposition time. The surface morphology and cross-sectional images were obtained by field-emission scanning electron microscopy (FESEM, S-4700, Hitachi, Japan), and the surface roughness was measured using an atomic force microscope (AFM, Dimension 3100, Veeco, USA). CIGAS films deposited on SLG were used for optical transmission and reflection measurements. The spectra were acquired in the wavelength range of 200–1200 nm using a double-beam UV/Vis spectrophotometer (LAMBDA 45, PerkinElmer, USA).

3 Results and discussion

Table 1 summarizes the chemical composition of as-deposited CIGAS thin films and the films annealed at 520 °C determined by EPMA. The Al content varies between 4.77 and 5.55 % while the Al/(Al + In + Ga) ratio remains nearly constant. In addition, there is no significant composition change before and after annealing. When compared to CIGS with the In and Ga contents of 15.2 and 6.2 % (data not shown in Table 1), respectively, it can be seen that the reduction of In content due to Al addition is more significant than the reduction of Ga content, an indication that Al mainly replaces In when incorporated into CIGS. It should be noted that the chemical composition of CIGS films deviated from that of the sputtering target probably due to the difference in sticking coefficient for different elements.

Table 1 Composition of as-deposited and annealed CIGAS films on Si(100)

Substrate temperature (°C)	Cu	In	Ga	Al	Se	Al/(Al + In + Ga)
25						
As-deposited	20.37	13.45	5.78	5.31	55.09	0.20
Annealed	20.93	14.25	5.79	4.98	54.05	0.20
150						
As-deposited	20.61	13.42	6.14	5.02	54.82	0.20
Annealed	20.80	13.64	5.98	4.77	54.81	0.20
250						
As-deposited	20.83	13.21	5.97	5.33	54.67	0.21
Annealed	20.96	13.33	6.00	5.17	54.54	0.21
350						
As-deposited	20.83	13.61	5.80	5.55	54.21	0.21
Annealed	20.95	13.53	5.87	5.30	54.36	0.21
500						
As-deposited	21.96	12.29	5.98	5.47	54.31	0.21
Annealed	21.53	13.06	6.04	5.20	54.17	0.21

To study the Al distribution across the film thickness, SIMS analysis was carried out on both as-deposited and annealed CIGAS films. The representative SIMS depth profiles are presented in Fig. 1. For comparison with CIGAS, SIMS depth profile of a CIGS film is shown in Fig. 1a. For as-deposited films, Al is clearly distributed non-uniformly across the film thickness with its concentration peaking in the middle where Al was deposited during sputtering. Moreover, at the high Al content region, both In and Ga concentrations decrease with In exhibiting more reduction, indicating that more In is replaced by Al. These results are also in good agreement with the EPMA

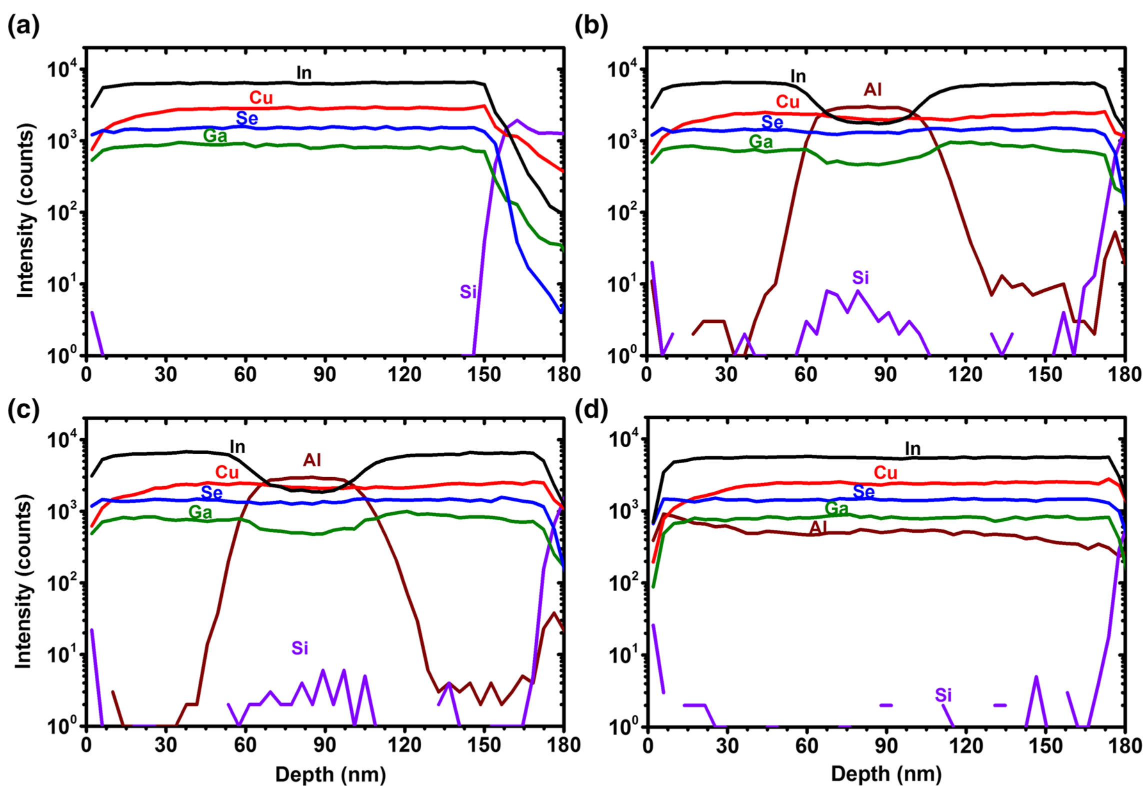

Fig. 1 SIMS depth profiles of Al, Ga, In, Cu, Se, and Si for CIGS and CIGAS thin films on Si(100): **a** CIGS deposited at 350 °C, **b** CIGAS deposited at 350 °C, **c** CIGAS deposited at 350 °C and subsequently annealed at 350 °C for 5 h, and **d** CIGAS deposited at 350 °C and subsequently annealed at 520 °C for 5 h

analysis. Figure 2c, d show SIMS profile of CIGAS films annealed for 5 h at 350 and 520 °C, respectively. It can be seen that the Al depth profile remains nearly unchanged when annealed at 350 °C. However, when the annealing temperature was increased to 520 °C, the Al distribution became nearly uniform across the film thickness and the concentration of In and Ga became uniform across the film thickness.

Figure 2a, b show the XRD patterns of as-deposited and annealed CIGAS films, respectively. The films exhibited pure chalcopyrite phase with their peaks identified using ICDD standards (PDF card No. 00-035-1102) for CIGS. As expected, the peak intensities increase with annealing, indicating improved crystallinity for all the films. It is also observed that the (112) peak shifts to higher 2θ values as the substrate temperature was increased, as shown in Fig. 2c. The reason for such shift may be two-fold. Firstly, the stress within the films during deposition is relieved with increasing substrate temperature, thus reducing the defects and promoting structure ordering [24]. Secondly, since the Al added into the as-deposited films is concentrated near the middle of the films (Fig. 1b), the measured XRD patterns result from mixed CIGS and CIGAS phases. Since Al mainly replaces In in CIGAS and the lattice constants of $CuAlSe_2$ are less than that of $CuInSe_2$ [25], alloying Al with CIGS would result in the (112) peak shift to higher 2θ values. Additionally, the FWHM of (112) peak decreases as the substrate temperature increases, as shown in Fig. 2c, which may be partially due to improved Al distribution with increasing substrate temperatures. In fact, the (112) peaks from CIGAS films annealed at 520 °C for 5 h do not show any shift, and their FWHM values are lower than those of as-deposited films.

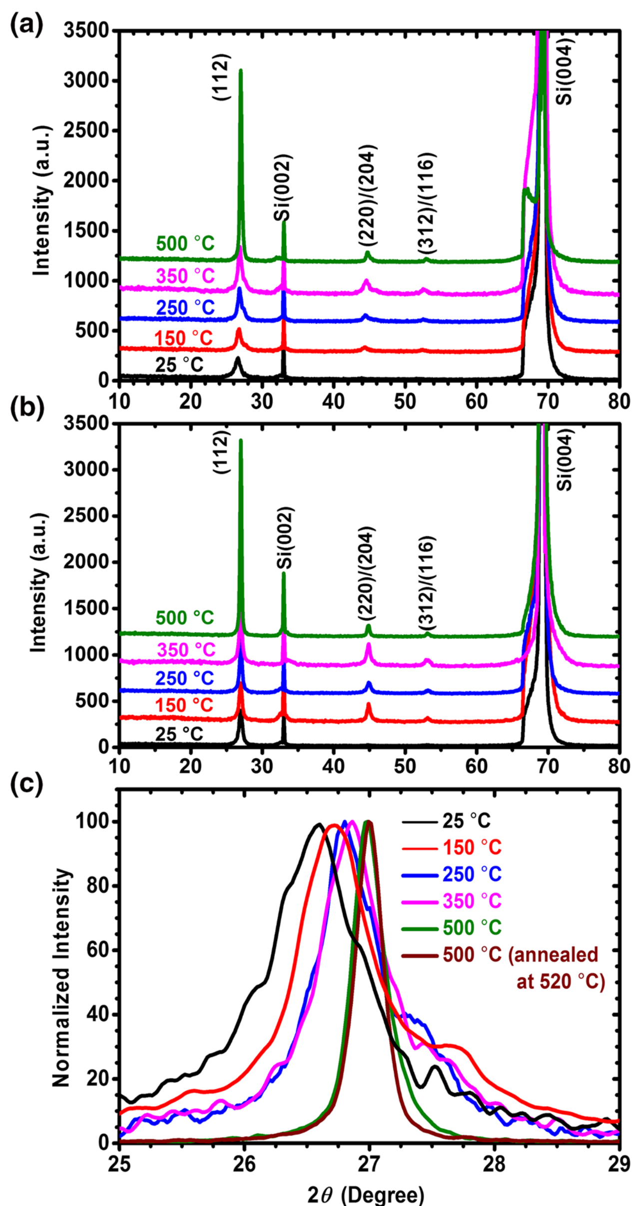

Fig. 2 XRD patterns of CIGAS thin films on Si(100): **a** as-deposited, **b** annealed at 520 °C for 5 h, and **c** normalized (112) peak for as-deposited films and for a film deposited at 500 °C and subsequently annealed at 520 °C for 5 h

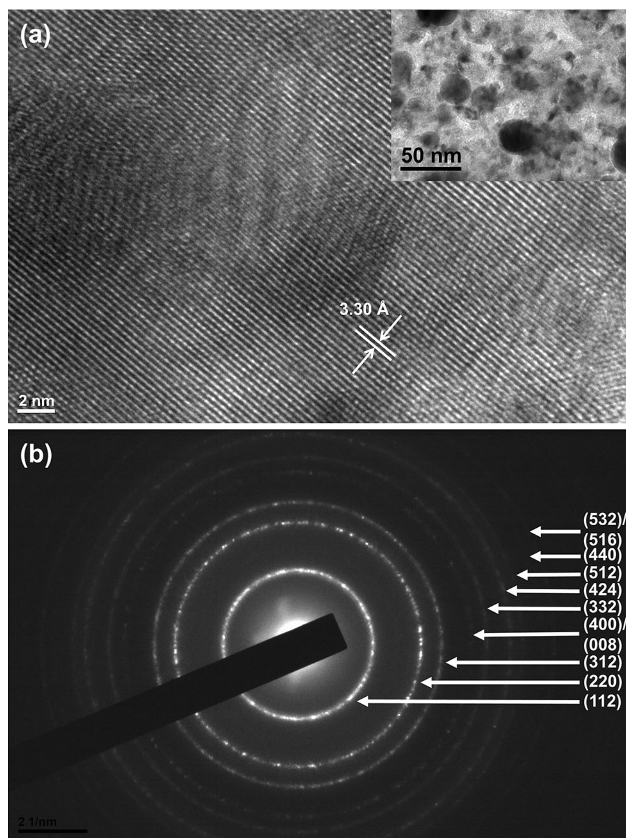

Fig. 3 **a** HRTEM image of a CIGAS thin film deposited at 500 °C. The *inset* is a low magnification HRTEM image. **b** SAD pattern with diffraction rings labeled indicating pure chalcopyrite structure

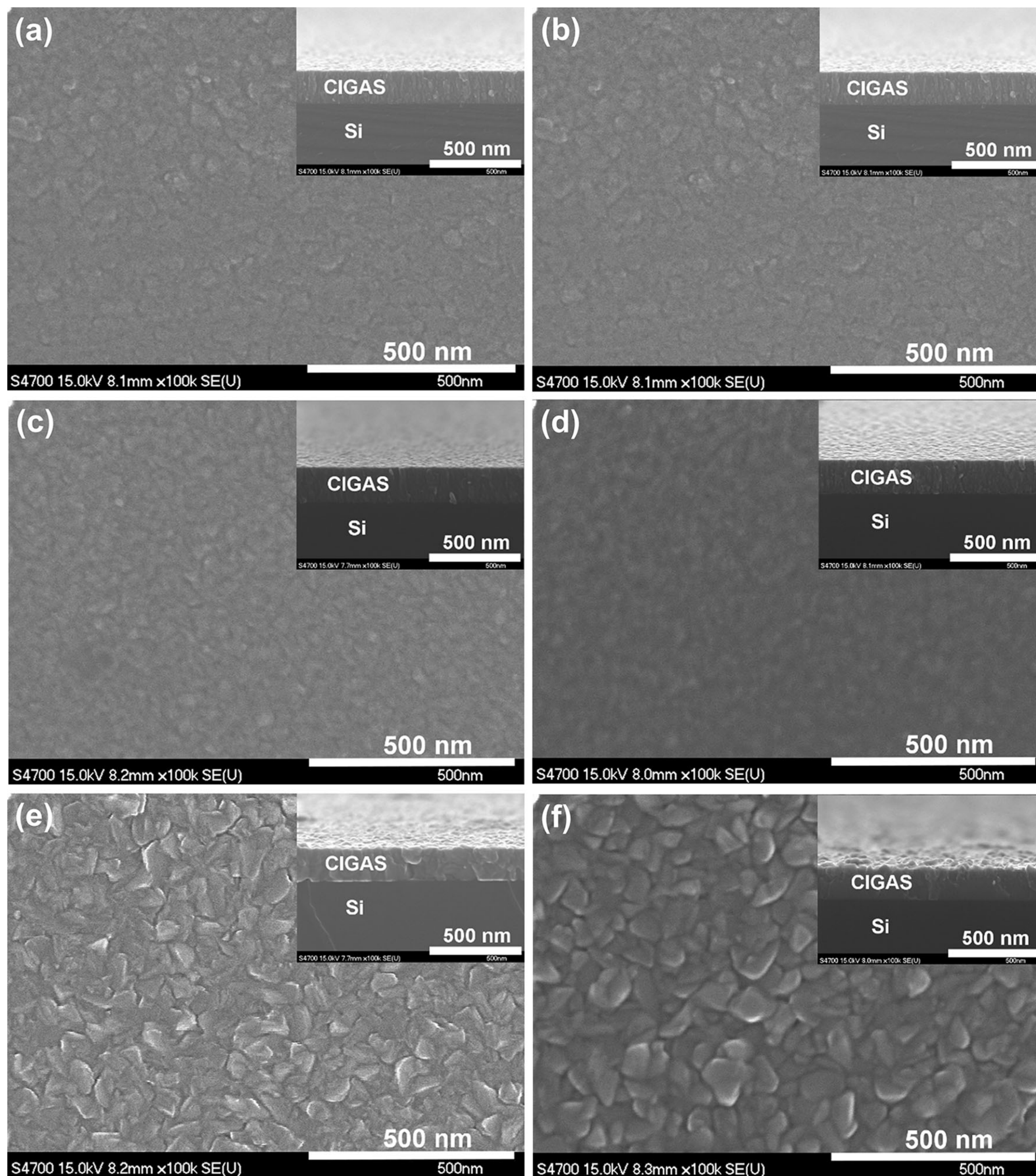

Fig. 4 FESEM images of CIGAS thin films deposited at **a** 250 °C, **c** 350 °C, and **e** 500 °C on Si(100). **b**, **d**, and **f** are the FESEM images of corresponding films annealed at 520 °C for 5 h. *Insets* are cross-sectional images for each film

Figure 3a shows the HRTEM images of a CIGAS film deposited at 500 °C without annealing. The measured interplanar spacing is 3.30 Å, which matches well with the $d_{(112)}$ value calculated from the XRD pattern obtained from films deposited under the same conditions. The inset of Fig. 3a is a low magnification TEM image revealing polycrystalline structure with grain size of a few tens of nanometers. Figure 3b shows a selected area diffraction (SAD) pattern acquired from the same sample with all diffraction rings identified and labeled using the ICDD PDF card No. 00-035-1102 for CIGS. These results indicate that the film has pure chalcopyrite phase, which is in good agreement with XRD data.

Figure 4a, c, and e show the surface and cross-sectional FESEM images of CIGAS thin films deposited at 250, 350 and 500 °C, respectively, and (b), (d), and (f) are the FESEM images of corresponding films subject to 520 °C post-deposition annealing. It can be clearly seen that the grains are much larger for the film deposited at 500 °C as compared to the other two films deposited at lower

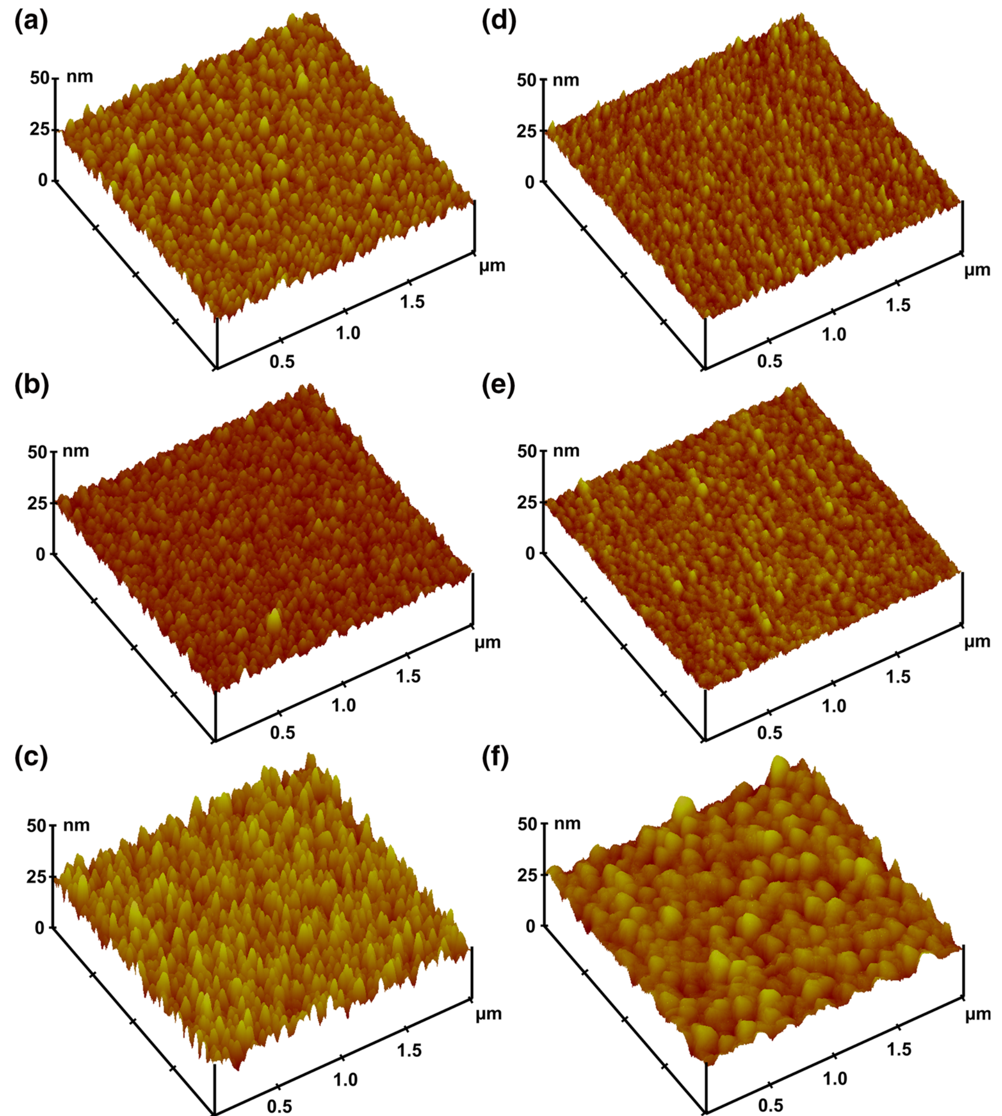

Fig. 5 AFM images of CIGAS thin films deposited at **a** 250 °C, **b** 350 °C, and **c** 500 °C on Si(100). **d**, **e**, and **f** are the AFM images of corresponding films annealed at 520 °C for 5 h

temperatures, which is an indication of significant grain growth at substrate temperatures of 500 °C or higher. Also, upon annealing, the surface morphologies of the CIGAS films remain mostly unchanged, although the grain boundaries of annealed films appear to be less sharp than those of as-deposited films. Moreover, the cross-sectional FESEM images (insets in Fig. 4) revealed columnar grains for both as-deposited and annealed films and sharp interfaces between CIGAS films and Si substrates. The film thickness is measured to be ~200 nm.

The surface morphologies of CIGAS films were further studied using AFM, and representative images are shown in Fig. 5. Similar to the increase in grain size for films deposited at 500 °C, as observed by FESEM, the measured root mean square (RMS) roughness also increases significantly from ~3 nm for films deposited at below 500 °C (Fig. 5a, b) to 6.0 nm for the film deposited at 500 °C (Fig. 5c). It was also observed that the RMS roughness decreases after the films were subject to post-deposition annealing at 520 °C for 5 h, i.e. ~1.7 nm for films deposited at below 500 °C (Fig. 5d, e) to 3.7 nm for the film deposited at 500 °C (Fig. 5f), which is also accompanied by diffusion of Al across the film thickness to form an almost uniform distribution. Similarly, Al incorporation into CIGS was observed to reduce the surface roughness with the RMS roughness values decreasing notably with the increase of Al content in pulsed laser deposited CIGAS films [11]. Such reduction in surface roughness may benefit the development of CIGAS-based solar cells since high surface roughness could result in an incomplete coverage by CdS buffer layer between p-CIGS and n-ZnO which could provide a shunt path [19].

The optical bandgap (E_g) of both as-deposited and 520 °C-annealed CIGAS films were determined using the

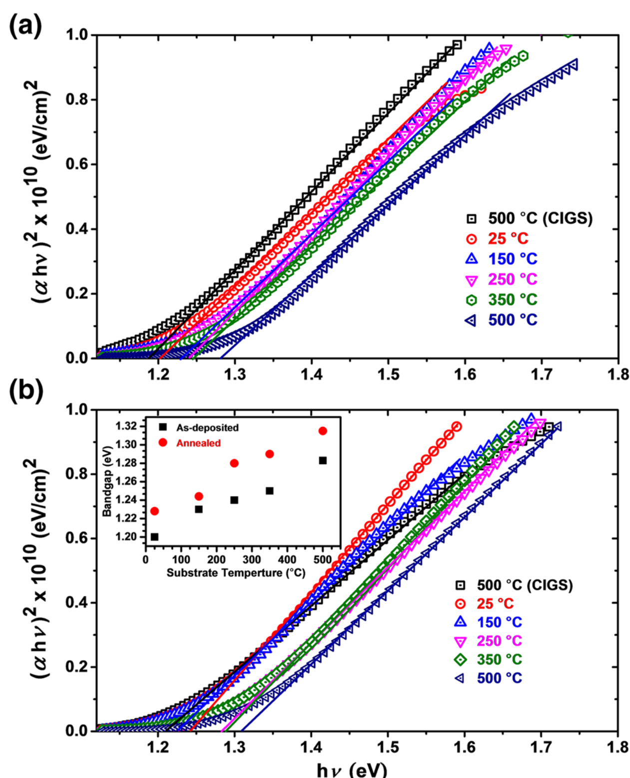

Fig. 6 $(\alpha h\upsilon)^2$ versus $h\upsilon$ plots for CIGS (noted in the plots) and CIGAS thin films on SLG: **a** as-deposited; **b** annealed at 520 °C for 5 h. The *inset* shows the bandgap change with varying substrate temperatures

optical data, including transmittance and reflectance spectra, acquired from films deposited on SLG substrates. The absorption coefficient (α) was calculated using the following equation [26]:

$$\alpha = \frac{1}{d}\ln\left[\frac{(1-R)^2}{2T} + \left(\frac{(1-R)^4}{4T^2} + R^2\right)^{1/2}\right], \quad (1)$$

where d is the film thickness, R is the reflectance, and T is the transmittance. Since chalcopyrite compounds are direct gap semiconductors, Tauc's equation can be applied [27]:

$$\alpha h\upsilon = A_a\left(h\upsilon - E_g\right)^{1/2}, \quad (2)$$

where A_a is a constant that depends on the transition nature, the effective mass, and the refractive index and $h\upsilon$ is the incident photon energy. Figure 6 shows the $(\alpha h\upsilon)^2$ versus $h\upsilon$ plots for as-deposited and annealed CIGAS thin films. The bandgap was then determined by extrapolating the linear portion of $(\alpha h\upsilon)^2$ versus $h\upsilon$ curve to the abscissa. For comparison, similar plots for a CIGS film deposited at 500 °C and subsequently annealed at 520 °C for 5 h are also included in Fig. 6a, b, respectively. As expected, the E_g values of both as-deposited and annealed CIGAS films are higher than those of corresponding CIGS films due to the addition of Al. Moreover, for as-deposited CIGAS films, the bandgap increases slightly from 1.20 to 1.28 eV as the substrate temperature was increased from room temperature to 500 °C. Such bandgap increase may be attributed to reduced structural imperfection and improved crystallinity [28], as evidenced by increased peak intensities of the XRD patterns (Fig. 2a). The bandgap for annealed CIGAS films also exhibited similar trend, as shown in Fig. 6b, but with higher E_g values, an indication of much improved Al distribution across film as well structure ordering upon annealing.

4 Conclusion

Polycrystalline CIGAS thin films with 5.3 % Al were deposited by magnetron sputtering at different substrate temperatures and then annealed at 520 °C for 5 h. SIMS depth profile revealed that for as-deposited films, Al concentration peaks in the middle region of the films where Al was sputtered. However, after annealing, the distribution of Al as well as In and Ga was much improved and became nearly uniform across the film thickness. XRD analysis showed that all films have pure chalcopyrite phase and the (112) peak shifts to higher 2θ values with decreasing FWHM values as the substrate temperature increases, which may be contributed to the non-uniform distribution of Al since such shift was not observed for the films annealed at 520 °C. Planar and cross-sectional FESEM images revealed dense and well-defined columnar grains for all films. The grain size exhibited significant increase for films deposited at 500 °C resulting in much higher surface roughness compared to films deposited below 500 °C. The optical bandgap of both as-deposited and annealed CIGAS films, determined from transmittance and reflectance spectra, also exhibited a shift to higher values as the substrate temperature was increased.

Acknowledgments This material is based upon work supported by the Virginia Center for Innovative Technology and the National Science Foundation under Grant Nos. MRI-0821180 and MRI-1428298. Talaat A. Hameed was supported by Egyptian Department of Mission. The authors thank the Surface Characterization Lab at The College of William & Mary for their help with FESEM analysis.

References

1. T. Sakurai, M.M. Islam, H. Uehigashi, S. Ishizuka, A. Yamada, K. Matsubara, S. Niki, K. Akimoto, Sol. Energy Mater. Sol. Cells **95**, 227 (2011)
2. M.A. Green, K. Emery, Y. Hishikawa, W. Warta, E.D. Dunlop, Prog. Photovolt. Res. Appl. **21**, 1 (2013)
3. M.A. Green, K. Emery, Y. Hishikawa, W. Warta, Prog. Photovolt. Res. Appl. **19**, 84 (2011)

4. S.M. Kong, R. Fan, S.H. Jung, C.W. Chung, J. Ind. Eng. Chem. **19**, 1320 (2013)
5. J.C. Mikkelsen, J. Electron. Mater. **10**, 541 (1981)
6. S. Jung, S. Ahn, J.H. Yun, J. Gwak, D. Kim, K. Yoon, Curr. Appl. Phys. **10**, 990 (2010)
7. M. Gossla, W.N. Shafarman, Thin Solid Films **480–481**, 33 (2005)
8. S. Marsillac, P.D. Paulson, M.W. Haimbodi, R.W. Birkmire, W.N. Shafarman, Appl. Phys. Lett. **81**, 1350 (2002)
9. W. Gebicki, M. Igalson, W. Zajac, R. Trykozko, J. Phys. D Appl. Phys. **23**, 964 (1990)
10. T.A. Hameed, W. Cao, B.A. Mansour, I.K. Elzawaway, E.M. Abdelrazek, H.E. Elsayed-Ali, J. Vac. Sci. Technol., A **33**, 031201 (2015)
11. W. Chen, W. Cao, T.A. Hameed, S. Marsillac, H.E. Elsayed-Ali, J. Mater. Sci. Mater. El. **26**, 1743 (2014)
12. M.L. Chenene, V. Alberts, J. Phys. D Appl. Phys. **36**, 56 (2003)
13. V. Probst F. Karg, H. Harms, J. Rimmasch, W. Riedl, J. Kotschy, J. Holz, R. Teichler, O. Eibl, A. Mittwalskyand, A. Kiend, in *Proceedings of the 23rd IEEE Photovoltaic Specialists Conference*, Louisville, KY, USA (1993)
14. S. Shirakata, Y. Kannaka, H. Hasegawa, T. Kariya, S. Isomura, Jpn. J. Appl. Phys. **38**, 4997 (1999)
15. R.N. Bhattacharya, J.F. Hiltner, W. Batchelor, M.A. Contreras, R.N. Noufi, J.R. Sites, Thin Solid Films **361–362**, 396 (2000)
16. A. Bouloufa, K. Djessas, D. Todorovic, Mat. Sci. Semicond. Proc. **12**, 82 (2009)
17. J.H. Shi, Z.Q. Li, D.W. Zhang, Q.Q. Liu, Z. Sun, S.M. Huang, Prog. Photovolt. Res. Appl. **19**, 160 (2011)
18. L. Oliveira, T. Todorov, E. Chassaing, D. Lincot, J. Carda, P. Escribano, Thin Solid Films **517**, 2272 (2009)
19. W.K. Metzger, I.L. Repins, M. Romero, P. Dippo, M. Contreras, R. Noufi, D. Levi, Thin Solid Films **517**, 2360 (2009)
20. P. Jackson, R. Würz, U. Rau, J. Mattheis, M. Kurth, T. Schlötzer, G. Bilger, J.H. Werner, Prog. Photovolt. Res. Appl. **15**, 507 (2007)
21. P. Jackson, D. Hariskos, E. Lotter, S. Paetel, R. Wuerz, R. Menner, W. Wischmann, M. Powalla, Prog. Photovolt. Res. Appl. **19**, 894 (2011)
22. K. Ellmer, J. Hinze, J. Klaer, Thin Solid Films **413**, 92 (2002)
23. Y. Yan, S. Li, Y. Ou, Y. Ji, C. Yan, L. Liu, Z. Yu, Y. Zhao, J. Mod. Transport. **22**, 37 (2014)
24. Y.H. Jo, B.C. Mohanty, Y.S. Cho, Appl. Surf. Sci. **256**, 6819 (2010)
25. E. Halgand, J.C. Bernède, S. Marsillac, J. Kessler, Thin Solid Films **480–481**, 443 (2005)
26. H. Neumann, W. Hörig, E. Reccius, W. Möller, G. Kühn, Solid State Commun. **27**, 449 (1978)
27. I.V. Pankove, *Optical Processes in Semiconductors* (Dover Inc, New York, 1971)
28. R.D. Tomlison, E. Ahmed, R.D. Pilkington, A.E. Hill, W. Ahmed, N. Ali, I.U. Hassan, Thin Solid Films **335**, 54 (1998)